



City Research Online

City, University of London Institutional Repository

Citation: Karim, M. R., Rahman, B. M. & Agrawal, G. P. (2015). Mid-infrared supercontinuum generation using dispersion-engineered $\text{Ge}_{11.5}\text{As}_{24}\text{Se}_{64.5}$ chalcogenide channel waveguide. *Optics Express*, 23(5), pp. 6903-6914. doi: 10.1364/oe.23.006903

This is the accepted version of the paper.

This version of the publication may differ from the final published version.

Permanent repository link: <https://openaccess.city.ac.uk/id/eprint/14400/>

Link to published version: <https://doi.org/10.1364/oe.23.006903>

Copyright: City Research Online aims to make research outputs of City, University of London available to a wider audience. Copyright and Moral Rights remain with the author(s) and/or copyright holders. URLs from City Research Online may be freely distributed and linked to.

Reuse: Copies of full items can be used for personal research or study, educational, or not-for-profit purposes without prior permission or charge. Provided that the authors, title and full bibliographic details are credited, a hyperlink and/or URL is given for the original metadata page and the content is not changed in any way.

City Research Online:

<http://openaccess.city.ac.uk/>

publications@city.ac.uk

Mid-infrared supercontinuum generation using dispersion-engineered $\text{Ge}_{11.5}\text{As}_{24}\text{Se}_{64.5}$ chalcogenide channel waveguide

M. R. Karim,^{1,*} B. M. A. Rahman,¹ and Govind P. Agrawal²

¹*School of Mathematics, Computer Science and Engineering, City University London, Northampton Square, London, EC1V 0HB, UK*

²*The Institute of Optics, University of Rochester, Rochester, New York, 14627, USA*

[*mohammad.karim.2@city.ac.uk](mailto:mohammad.karim.2@city.ac.uk)

Abstract: We numerically investigate mid-infrared supercontinuum (SC) generation in dispersion-engineered, air-clad, $\text{Ge}_{11.5}\text{As}_{24}\text{Se}_{64.5}$ chalcogenide-glass channel waveguides employing two different materials, $\text{Ge}_{11.5}\text{As}_{24}\text{S}_{64.5}$ or MgF_2 glass for their lower cladding. We study the effect of waveguide parameters on the bandwidth of the SC at the output of 1-cm-long waveguide. Our results show that output can vary over a wide range depending on its design and the pump wavelength employed. At the pump wavelength of $2\ \mu\text{m}$ the SC never extended beyond $4.5\ \mu\text{m}$ for any of our designs. However, supercontinuum could be extended to beyond $5\ \mu\text{m}$ for a pump wavelength of $3.1\ \mu\text{m}$. A broadband SC spanning from $2\ \mu\text{m}$ to $6\ \mu\text{m}$ and extending over 1.5 octave could be generated with a moderate peak power of 500 W at a pump wavelength of $3.1\ \mu\text{m}$ using an air-clad, all-chalcogenide, channel waveguide. We show that SC can be extended even further when MgF_2 glass is used for the lower cladding of chalcogenide waveguide. Our numerical simulations produced SC spectra covering the wavelength range $1.8\text{--}7.7\ \mu\text{m}$ ($>$ two octaves) by using this geometry. Both ranges exceed the broadest SC bandwidths reported so far. Moreover, we realize it using $3.1\ \mu\text{m}$ pump source and relatively low peak power pulses. By employing the same pump source, we show that SC spectra can cover a wavelength range of $1.8\text{--}11\ \mu\text{m}$ ($>$ 2.5 octaves) in a channel waveguide employing MgF_2 glass for its lower cladding with a moderate peak power of 3000 W.

© 2016 Optical Society of America

OCIS codes: (000.4430) Numerical approximation and analysis; (130.2755) Glass waveguides; (190.4390) Nonlinear optics, devices; (320.6629) Dispersion; (320.6629) Supercontinuum generation.

References and links

1. X. Gai, T. Han, A. Prasad, S. Madden, D. Y. Choi, R. Wang, D. Bulla, and B. Luther-Davies, "Progress in optical waveguides fabricated from chalcogenide glasses," *Opt. Express* **18**(25), 26635–26646 (2010).
2. J. Hu, C. R. Menyuk, L. B. Shaw, J. S. Sanghera, and I. D. Aggarwal, "Maximizing the bandwidth of supercontinuum generation in As_2Se_3 chalcogenide fibers," *Opt. Express* **18**(3), 6722–6739 (2010).
3. I. D. Aggarwal and J. S. Sanghera, "Development and applications of chalcogenide glass optical fibers at NRL," *J. Optoelectron. Adv. Mater.* **4**(3), 665–678 (2002).

4. B. J. Eggleton, B. Luther-Davies, and K. Richardson, "Chalcogenide photonics," *Nat. Photonics* **5**, 141–148 (2011).
5. F. Luan, M. D. Pelusi, M. R. E. Lamont, D. Y. Choi, S. J. Madden, B. Luther-Davies, and B. J. Eggleton, "Dispersion engineered As₂S₃ planar waveguides for broadband four-wave mixing based wavelength conversion of 49 Gb/s signals," *Opt. Express* **17**(5), 3514–3520 (2009).
6. S. J. Madden, D. Y. Choi, D. A. Bulla, A. V. Rode, B. Luther-Davies, V. G. Ta'eed, M. D. Pelusi, and B. J. Eggleton, "Long, low loss etched As₂S₃ chalcogenide for all-optical signal regeneration," *Opt. Express* **15**(22), 14414–14421 (2007).
7. M. R. E. Lamont, C. M. Sterke, and B. J. Eggleton, "Dispersion engineering of highly nonlinear As₂S₃ waveguides for parametric gain and wavelength conversion," *Opt. Express* **15**(15), 9458–9463 (2007).
8. M. R. Karim, B. M. A. Rahman, and G.P. Agrawal, "Dispersion engineered Ge_{11.5}As₂₄Se_{64.5} nanowire for supercontinuum generation: A parametric study," *Opt. Express* **22**(25), 31029–31040 (2014).
9. D. D. Hudson, E. C. Mägi, A. C. Judge, S. A. Dekker, and B. J. Eggleton, "Highly nonlinear chalcogenide glass micro/nanofiber devices: Design, theory, and octave-spanning spectral generation," *Opt. Commun.* **285**, 4660–4669 (2012).
10. P. Ma, D. Y. Choi, Y. Yu, X. Gai, Z. Yang, S. Debbarma, S. Madden, and B. Luther-Davies, "Low-loss chalcogenide waveguides for chemical sensing in the mid-infrared," *Opt. Express* **21**(24), 29927–29937 (2013).
11. M. R. E. Lamont, B. Luther-Davies, D. Y. Choi, S. Madden, and B. J. Eggleton, "Supercontinuum generation in dispersion engineered highly nonlinear ($\gamma = 10$ /W/m) As₂S₃ chalcogenide planar waveguide," *Opt. Express* **16**(19), 14938–14944 (2008).
12. X. Gai, S. Madden, D. Y. Choi, D. Bulla, and B. Luther-Davies, "Dispersion engineered Ge_{11.5}As₂₄Se_{64.5} nanowires with a nonlinear parameter of 136 W⁻¹m⁻¹ at 1550 nm," *Opt. Express* **18**(18), 18866–18874 (2010).
13. X. Gai, D. Choi, S. Madden, Z. Yang, R. Wang, and B. Luther-Davies, "Supercontinuum generation in the mid-infrared from a dispersion-engineered As₂S₃ glass rib waveguide," *Opt. Lett.* **37**(18), 3870–3872 (2012).
14. Y. Yu, X. Gai, T. Wang, P. Ma, R. Wang, Z. Yang, D. Choi, S. Madden, and B. Luther-Davies, "Mid-infrared supercontinuum generation in chalcogenides," *Opt. Express* **3**(8), 1075–1086 (2013).
15. Y. Yu, X. Gai, P. Ma, D. Choi, Z. Yang, R. Wang, S. Debbarma, S. J. Madden, and B. Luther-Davies, "A broadband, quasi-continuous, mid-infrared supercontinuum generated in a chalcogenide glass waveguide," *Laser Photonics Rev.*, 1–7 (2014).
16. R. J. Weiblen, A. Docherty, J. Hu, and C. R. Menyuk, "Calculation of the expected bandwidth for a mid-infrared supercontinuum source based on As₂S₃ chalcogenide photonic crystal fibers," *Opt. Express* **18**(25), 26666–26674 (2010).
17. L. B. Shaw, R. R. Gattass, J. S. Sanghera, and I. D. Aggarwal, "All-fiber mid-IR supercontinuum source from 1.5 to 5 μ m," *Proc. SPIE* **7914** (79140P), 1–5 (2011).
18. A. Marandi, C. W. Rudy, V. G. Plotnichenko, E. M. Dianov, K. L. Vodopyanov, and R. L. Byer, "Mid-infrared supercontinuum generation in tapered chalcogenide fiber for producing octave spanning frequency comb around 3 μ m," *Opt. Express* **20**(22), 24218–24225 (2012).
19. I. Savellii, O. Mouawad, J. Fatome, B. Kibler, F. Desevedavy, G. Gadret, J. C. Jules, P. Y. Bony, H. Kawashima, W. Gao, T. Kohoutek, T. Suzuki, Y. Ohishi, and F. Smektala, "Mid-infrared 2000-nm bandwidth supercontinuum generation in suspended-core microstructured Sulphide and Tellurite optical fibers," *Opt. Express* **20**(24), 27083–27093 (2012).
20. W. Gao, M. E. Amraoui, M. Liao, H. Kawashima, Z. Duan, D. Deng, T. Cheng, T. Suzuki, Y. Messaddeq, and Y. Ohishi, "Mid-infrared supercontinuum generation in a suspended-core As₂S₃ chalcogenide microstructured optical fiber," *Opt. Express* **21**(8), 9573–9583 (2013).
21. N. Granzow, M.A. Schmidt, W. Chang, L. Wang, Q. Coulombier, J. Troles, P. Toupin, I. Hartl, K. F. Lee, M. E. Fermann, L. Wondraczek, and P. St. J. Russell, "Mid-infrared supercontinuum generation in As₂S₃ "nano-spike" step index waveguide," *Opt. Express* **21**(9), 10969–10977 (2013).
22. C. Wei, X. Zhu, R. A. Norwood, F. Seng, and N. Peyghambarian, "Numerical investigation on high power mid-infrared supercontinuum fiber lasers pumped at 3 μ m," *Opt. Express* **21**(24), 29488–29504 (2013).
23. I. Kubat, C. R. Petersen, U. V. Moller, A. B. Seddon, T. M. Benson, L. Brilland, D. Mechin, P. M. Moselund, and O. Bang, "Thulium pumped mid-infrared 0.9-9 μ m supercontinuum generation in concatenated fluoride and chalcogenide glass fibers," *Opt. Express* **22**(4), 3959–3967 (2014).
24. I. Kubat, C. S. Agger, U. Moller, A. B. Seddon, Z. Tang, S. Sujecki, T. M. Benson, D. Furniss, S. Lamarini, K. Scholle, P. Fuhrberg, B. Napier, M. Farries, J. Ward, P. M. Moselund, and O. Bang, "Mid-infrared supercontinuum generation to 12.5 μ m in large NA chalcogenide step-index fibers pumped at 4.5 μ m," *Opt. Express* **22**(16), 19169–19182 (2014).
25. D. D. Hudson, M. Baudisch, D. Werdehausen, B. J. Eggleton, and J. Biegert, "1.9 octave supercontinuum generation in a As₂S₃ step-index fiber driven by mid-IR OPCPA," *Opt. Lett.* **39**(19), 5752–5755 (2014).
26. A. Al-Kadry, M. E. Amraoui, Y. Messaddeq, and M. Rochette, "Two octaves mid-infrared supercontinuum generation in As₂Se₃ microwires," *Opt. Express* **22**(25), 31131–31137 (2014).
27. C. R. Petersen, U. Møller, I. Kubat, B. Zhou, S. Dupont, J. Ramsay, T. Benson, S. Sujecki, M. Abdel-Moneim, Z. Tang, D. Furniss, A. Seddon, and O. Bang, "Mid-infrared supercontinuum covering the 1.4–13.3 μ m molecular

- fingerprint region using ultra-high NA chalcogenide step-index fibre,” *Nat. Photonics* **8**, 830–834 (2014).
28. U. Møller, Y. Yu, I. Kubat, C. R. Petersen, X. Gai, L. Brilland, D. Mechin, C. Caillaud, J. Troles, B. Luther-Davies, and O. Bang, “Multi-milliwatt mid-infrared supercontinuum generation in a suspended core chalcogenide fiber,” *Opt. Express* **23**(3), 3282–3291 (2015).
 29. J. H. Kim, M. Chen, C. Yang, J. Lee, S. Yin, P. Ruffin, E. Edwards, C. Brantley, and C. Luo, “Broadband IR supercontinuum generation using single crystal sapphire fibers,” *Opt. Express* **16**(6), 4085–4093 (2008).
 30. B. Kuyken, X. Liu, R. M. Osgood Jr., R. Baets, G. Roelkens, and W. M. J. Green, “Mid-infrared to telecom-band supercontinuum generation in highly nonlinear silicon-on-insulator wire waveguides,” *Opt. Express* **19**(21), 20172–20181 (2011).
 31. O. P. Kulkarni, V. V. Alexander, M. Kumar, M. J. Freeman, M. N. Islam, F. L. Terry Jr., M. Neelakandan, and A. Chan “Supercontinuum generation from 1.9 to 4.5 μm in ZBLAN fiber with high average power generation beyond 3.8 μm using a thulium-doped fiber amplifier,” *J. Opt. Soc. Am. B* **28**(10), 2486–2498 (2011).
 32. M. Liao, W. Gao, T. Cheng, X. Xue, Z. Duan, D. Deng, H. Kawashima, T. Suzuki, and Y. Ohishi, “Five-octave-spanning supercontinuum generation in fluoride glass,” *App. Phy. Exp.* **6**(032503) 1–3 (2013).
 33. E. A. Anashkina, A. V. Andrianov, M. Y. Koptev, S. V. Muravyev, and A. V. Kim, “Towards mid-infrared supercontinuum generation with germano-silicate fibers,” *IEEE J. of Sel. Top. in Quan. Elect.* **20** (5), 7600608 (2014).
 34. M. Bass, G. Li, and E. V. Stryland, *Hand Book of Optics Vol-IV 3rd ed.* (The McGraw-Hill, New York, 2010).
 35. D. Yeom, E. C. Mägi, M. R. E. Lamont, M. A. F. Roelens, L. Fu, and B. J. Eggleton, “Low-threshold supercontinuum generation in highly nonlinear chalcogenide nanowires,” *Opt. Lett.* **33**(7), 660–662 (2008).
 36. D. D. Hudson, S. A. Dekker, E. C. Mägi, A. C. Judge, S. D. Jackson, E. Li, J. S. Sanghera, L. B. Shaw, I. D. Aggarwal, and B. J. Eggleton, “Octave spanning supercontinuum in an As_2S_3 taper using ultralow pump pulse energy,” *Opt. Lett.* **36**(7), 1122–1124 (2011).
 37. G. P. Agrawal, *Nonlinear Fiber Optics 5th ed.* (Academic, San Diego, California, 2013).
 38. J. M. Dudley and J. R. Taylor, “Ten years of nonlinear optics in photonic crystal fiber,” *Nat. Photonics* **3**, 85–90 (2009).
 39. J. Andreasen, A. Bhal, and M. Kolesik, “Spatial effects in supercontinuum generation in waveguides,” *Opt. Express* **22**(21), 25756–25767 (2014).
 40. C. Chaudhari, T. Suzuki, and Y. Ohishi “Design of zero chromatic dispersion chalcogenide As_2S_3 glass nanofibers,” *J. Lightwave Technol.* **27**(12), 2095–2099, (2009).
 41. C. Chaudhari, M. Liao, T. Suzuki, and Y. Ohishi, “Chalcogenide core tellurite cladding composite microstructured fiber for nonlinear applications,” *J. Lightwave Technol.* **30**(13), 2069–2076, (2012).
 42. B. M. A. Rahman and J. B. Davies, “Finite-element solution of integrated optical waveguides,” *J. Lightwave Technol.* **2**(5), 682–688, (1984).
 43. N. Granzow, S. P. Stark, M. A. Schmidt, A. S. Tverjanovich, L. Wondraczek, and P. St. J. Russell, “Supercontinuum generation in chalcogenide-silica step-index fibers,” *Opt. Express* **19**(21), 21003–21010 (2011).
 44. B. M. A. Rahman and J. B. Davies, “Vector- H finite element solution of GaAs/GaAlAs rib waveguides,” in proceedings of IEE **132**(6), 349–353 (1985).
 45. F. Silva, D. R. Austin, A. Thai, M. Baudisch, M. Hemmer, D. Faccio, A. Couairon, and J. Biegert, “Multi-octave supercontinuum generation from mid-infrared filamentation in a bulk crystal” *Nat. Commun.* **3**(807), 1–5 (2012).
 46. D. V. Skryabin, F. Laun, J. C. Knight, and P. St. J. Russel, “Soliton self-frequency shift cancellation in photonic crystal fibers,” *Science*, **301**, 1705–1708 (2003).
 47. F. Biancalana, D. V. Skryabin, and A. V. Yulin, “Theory of the soliton self-frequency shift compensation by resonant radiation in photonic crystal fibers,” *Physical Review E*, **70**, 016615 (2004).
-

1. Introduction

Recently chalcogenide glasses (ChGs) have emerged as promising nonlinear materials having a number of unique properties that makes them attractive for fabricating planar optical waveguides and using them for application such as mid-infrared (MIR) supercontinuum (SC) generation and optical sensing [1]. SC generation in MIR has increasingly become a focus for research because bright MIR light sources can be used for molecular fingerprint spectroscopy, frequency metrology, optical coherent tomography and microscopy [2,3]. Chalcogenide glasses can provide MIR transparency with sulphides transmitting to beyond 8.5 μm , selenides to 14 μm and tellurites to around 20 μm [4]. A major advantage of chalcogenide glasses is their large ultra-fast nonlinearity amongst all glasses, making them good materials for planar waveguides to generate SC in the MIR [5–9]. A few of these ChG materials such as As_2S_3 , As_2Se_3 , $\text{Ge}_{11.5}\text{As}_{24}\text{Se}_{64.5}$ and $\text{Ge}_{11.5}\text{As}_{24}\text{Se}_{64.5}$ glasses are highly suitable for making active and passive devices in the MIR region. Amongst them $\text{Ge}_{11.5}\text{As}_{24}\text{Se}_{64.5}$ glass has excellent film-forming

properties with high thermal and optical stability under intense illumination [10]. Recently interest has grown in designing and optimizing planar waveguides made from $\text{Ge}_{11.5}\text{As}_{24}\text{Se}_{64.5}$ chalcogenide glass for broadband MIR SC generation with suitably tailored group-velocity dispersion (GVD), including a zero-dispersion wavelength (ZDW) close to the central wavelength of the pump [11, 12].

In recent years, several experimental and theoretical investigations on mid-infrared SC generation were reported in ChG planar waveguides [13–15], ChG fibers [16–28], single crystal sapphire fibers [29], silicon-on-insulator (SOI) wire waveguides [30], ZBLAN fiber [31], fluoride glass [32] and germano-silicate fibers [33]. Gai *et al.* [13] reported SC generation from 2.9 μm to 4.2 μm in dispersion-engineered As_2S_3 glass rib waveguide (6.6 cm long) pumped with 7.5 ps duration pulses at a wavelength of 3.26 μm with a pulse peak power of around 2 kW. Yu *et al.* [14] reported SC generation up to 4.7 μm using a 4.7-cm-long As_2S_3 glass rib waveguide employing MgF_2 glass as a substrate and pumped with 7.5 ps duration with a peak power of 1 kW pulses at a wavelength of 3.26 μm . They observed a flat SC extending from 2.5 μm to 7.5 μm in 5-mm-thick bulk sample of $\text{Ge}_{11.5}\text{As}_{24}\text{Se}_{64.5}$ glass pumped with 150 fs duration pulses with up to 20 MW peak power at a wavelength of 5.3 μm . They also reported theoretically that SC could be generated beyond 10 μm in a dispersion-engineered all-chalcogenide $\text{Ge}_{11.5}\text{As}_{24}\text{Se}_{64.5}$ glass rib waveguide pumped with 250 fs duration pulses at a wavelength of 4 μm or longer. Yu *et al.* [15] recently reported the generation of broadband SC spanning from 1.8 μm to 7.5 μm in dispersion-engineered $\text{Ge}_{11.5}\text{As}_{24}\text{Se}_{64.5}$ glass 1-cm-long rib waveguide pumped at 4 μm using 320 fs pulses from a periodically-poled lithium niobate optical parametric amplifier pumped with commercially available mode-locked Yb laser with a peak power of 3260 W. For step-index fiber based on As_2S_3 , Hudson *et al.* [25] reported 1.9-octave SC extending from 1.6 μm to 5.9 μm pumped at a wavelength of 3.1 μm with a peak power of 520 kW. Al-Kadry *et al.* [26] reported MIR SC generation from 1.1 μm to 4.4 μm in 10-cm-long As_2Se_3 microwires pumped with 800 fs duration pulses at a wavelength of 1.94 μm with energy of 500 pJ. Petersen *et al.* [27] used 100 fs pulses at 6.3 μm to generate SC covering the range 1.4–13.3 μm in 85 mm long As_2S_3 step-index fiber with a 16 μm core. Møller *et al.* [28] used a 18 cm long, low-loss, suspended core $\text{As}_{38}\text{S}_{62}$ fiber and generated a SC spanning from 1.7 to 7.5 μm by pumping this fiber with 320 fs pulses with a peak power of 5.2 kW at a wavelength of 4.4 μm . The SC generation in As_2S_3 fibers and waveguides has been limited to 5 μm due to their increased losses in the long wavelength region [13, 17, 18]. Although As_2Se_3 chalcogenide glass has its loss edge in the long wavelength region around 16–17 μm , the use of such materials for SC generation has so far been limited owing to high peak power pump sources required in the MIR region [4, 26, 27].

In this paper, we demonstrate numerically that a 1-cm-long dispersion-engineered $\text{Ge}_{11.5}\text{As}_{24}\text{Se}_{64.5}$ glass rectangular channel waveguide can generate broadband SC in the MIR regime. In our previous work [8], a dispersion-engineered $\text{Ge}_{11.5}\text{As}_{24}\text{Se}_{64.5}$ nanowire was designed, with polymer as top and silica as bottom claddings, for low-power wideband SC generation. To extend the SC to the MIR region and to ensure that the claddings as well as the core materials are transparent at such long wavelengths, rectangular channel waveguides were designed with air on top and either $\text{Ge}_{11.5}\text{As}_{24}\text{S}_{64.5}$ or MgF_2 glass as the lower cladding material. To tailor the dispersion to obtain the ZDW close to the pump wavelength, two separate geometries were employed, one with a lower cladding of $\text{Ge}_{11.5}\text{As}_{24}\text{S}_{64.5}$ glass having lower index contrast and another with a lower cladding of MgF_2 glass having larger index contrast. Both were designed and optimized by adjusting the waveguides dimensions. In earlier experiments it was found that the extension of SC depends on the pump wavelength, among many other factors. To achieve sufficiently long wavelength extension in MIR region, the pump wavelength will need to be used around 4–5 μm or longer. The nonlinear parameter, $\gamma = 2\pi n_2 / \lambda A_{\text{eff}}$, where

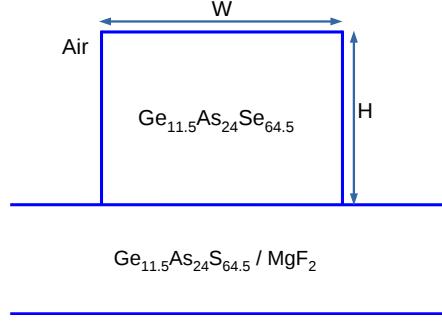


Fig. 1. Waveguide geometry.

n_2 is the nonlinear refractive index and A_{eff} is the effective area of the mode, of the ChG waveguide decreases with the increasing pump wavelength, λ . As A_{eff} also increases, high pump powers would be required to generate SC in the long-wavelength region, which can cause damage to the ChG waveguides if relatively wider pump pulses are employed [14]. For this reason we choose, for our numerical simulation, sub-picosecond pulses of 85 fs (FWHM) duration at a pump wavelength of $3.1 \mu\text{m}$ with a repetition rate of 160 kHz [45] and with low to moderate peak powers. The propagation loss (α) and nonlinear refractive index (n_2) were taken to be 0.5 dB/cm and $4.3 \times 10^{-18} \text{ m}^2/\text{W}$, respectively [10, 15]. Since the actual n_2 of ChG glasses has not been measured in the MIR region, its measured value at $1.55 \mu\text{m}$ [12] was reduced by a factor of two at the pump wavelength of $3.1 \mu\text{m}$ [15].

We carry out simulations for two different structures of ChG channel waveguides assuming that the input pulse excites the fundamental quasi-TE mode. The peak power varies in the range of 25-500 W and 100-3000 W for two pump sources at wavelength of $2 \mu\text{m}$ and $3.1 \mu\text{m}$, respectively. Using the pump source at $2 \mu\text{m}$ with a peak power of 500 W, the SC bandwidth extended in the range $1.3\text{-}3.3 \mu\text{m}$ and $1.3\text{-}3.5 \mu\text{m}$ for the waveguides designed and optimized with $\text{Ge}_{11.5}\text{As}_{24}\text{S}_{64.5}$ glass or MgF_2 glass acting as lower cladding, respectively. A broadband MIR SC extending over 1.5 octave from $2 \mu\text{m}$ to $6 \mu\text{m}$ could be generated with a lower cladding of $\text{Ge}_{11.5}\text{As}_{24}\text{S}_{64.5}$ glass. The SC extended over more than 2 octave ($1.8 \mu\text{m}$ to $7.7 \mu\text{m}$) when a lower cladding of MgF_2 glass was employed. We calculate the SC bandwidth at the -30 dB level from the peak. Our calculated bandwidths are the largest reported so far for SC generated using chalcogenide glass waveguides pumped at a wavelength of $3.1 \mu\text{m}$ with a moderate peak power of 500 W.

2. Theory

The schematic diagram of the $\text{Ge}_{11.5}\text{As}_{24}\text{Se}_{64.5}$ chalcogenide glass channel waveguide used in our simulations is shown in Fig. 1. The wavelength-dependent linear refractive index of $\text{Ge}_{11.5}\text{As}_{24}\text{Se}_{64.5}$, $\text{Ge}_{11.5}\text{As}_{24}\text{S}_{64.5}$ and MgF_2 glasses over the entire wavelength range used in the simulation was obtained using the Sellmeier equation,

$$n(\lambda) = \sqrt{1 + \sum_{j=1}^m \frac{A_j \lambda^2}{\lambda^2 - \lambda_j^2}}, \quad (1)$$

Here λ is the wavelength in micrometers. We use the Sellmeier coefficients calculated by fitting smooth curves to the measured refractive index data for the ChGs [10] and the MgF_2 [34] glasses. The values of the integer m and the fitting coefficients are given in Table 1.

Table 1. Sellmeier fitting coefficients

Material	Ge _{11.5} As ₂₄ Se _{64.5} [10]		Ge _{11.5} As ₂₄ S _{64.5} [10]		MgF ₂ [34]	
m	2		2		3	
	A_j	λ_j	A_j	λ_j	A_j	λ_j
$j = 1$	5.78525	0.28795	4.18011	0.31679	0.48755708	0.0433840
$j = 2$	0.39705	30.39338	0.35895	22.77018	0.39875031	0.09461442
$j = 3$					2.3120353	23.793604

Dispersion of the waveguide plays an important role in determining the SC spectrum. Ideally the dispersion near the pump wavelength should be anomalous with a small value that does not change much [35–40]. Small flattened anomalous dispersion with high nonlinearity is required for large frequency shifts of the Raman soliton. ChG glasses generally have smaller material dispersion than silicon and to obtain the ZDW close to the pump wavelength, relatively larger waveguide dispersion is required to offset the material dispersion [12, 41]. We use a finite element (FE) based mode-solver [42] to obtain the propagation constant $\beta(\omega)$ of the fundamental mode over a range of frequencies and calculate the effective index, $n_{\text{eff}} = \lambda\beta(\omega)/2\pi$ from this $\beta(\omega)$, which is subsequently used for numerically calculating the GVD parameter, $D(\lambda) = -\frac{\lambda}{c} \frac{d^2 n_{\text{eff}}}{d\lambda^2}$ (ps/nm/km) as well as all other higher-order dispersion parameters. Spectral broadening of a SC mainly depends on these dispersion parameters and the nonlinear coefficient, γ which in turn depends on the nonlinear refractive index of the material, n_2 and effective mode area of the waveguide. Pump wavelength is also an important factor for the extension of SC spectrum in the long wavelength region. Optimized mode area, A_{eff} can be obtained with our FE mode-solver and γ of the waveguide can be calculated using A_{eff} .

The FE approach used here is based on the vector- \mathbf{H} -field formulation, since it is one of the most accurate and numerically efficient approaches to obtain the modal field profiles and mode propagation constants $\beta(\omega)$ of various quasi-TE and quasi-TM modes. The full-vectorial formulation is based on the minimization of the full \mathbf{H} -field energy functional [42],

$$\omega^2 = \frac{\iint \left[(\nabla \times \mathbf{H})^* \cdot \hat{\epsilon}^{-1} (\nabla \times \mathbf{H}) + p (\nabla \cdot \mathbf{H})^* (\nabla \cdot \mathbf{H}) \right] dx dy}{\iint \mathbf{H}^* \cdot \hat{\mu} \mathbf{H} dx dy}, \quad (2)$$

where \mathbf{H} is the full-vectorial magnetic field, $*$ denotes a complex conjugate and transpose, ω^2 is the eigenvalue (ω being the angular frequency), p is a weighting factor for the penalty term to eliminate spurious modes and $\hat{\epsilon}$ and $\hat{\mu}$ are the permittivity and permeability tensors, respectively. The two-dimensional cross-section of the waveguide is discretized by using a large number of triangular elements. All three components of the magnetic fields can be represented as piece-wise polynomials within the elements. With a proper choice of waveguide discretization we can accurately calculate the energy functional by integrating it over each element.

To study SC generation in the MIR region, simulations were performed using a generalized nonlinear Schrödinger equation (GNLSE) for the slowly varying envelope of the pulse [8, 12]:

$$\begin{aligned} \frac{\partial}{\partial z} A(z, T) = & -\frac{\alpha}{2} A + \sum_{k \geq 2} \frac{i^{k+1}}{k!} \beta_k \frac{\partial^k A}{\partial T^k} + i \left(\gamma + i \frac{\alpha_2}{2A_{\text{eff}}} \right) \left(1 + \frac{i}{\omega_0} \frac{\partial}{\partial T} \right) \\ & \times \left(A(z, T) \int_{-\infty}^{\infty} R(T) |A(z, T - T')|^2 dT' \right), \end{aligned} \quad (3)$$

where A is the electrical field amplitude, α is the linear propagation loss of the waveguide,

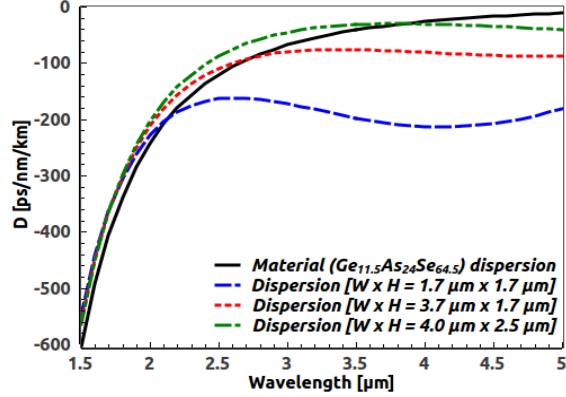


Fig. 2. GVD curves for the fundamental quasi-TE mode calculated from n_{eff} for three waveguide geometries employing $\text{As}_{36}\text{S}_{64}$ glass for both the upper and lower claddings. The black solid line curve shows the material dispersion curve for comparison.

$\beta_k(\omega) = \left. \frac{d^k \beta}{d\omega^k} \right|_{\omega=\omega_0}$ ($k \geq 2$) is the k^{th} order dispersion parameter, and $T = t - \frac{z}{v_g}$ is the retarded time frame moving with the group velocity $v_g = \frac{1}{\beta_1(\omega_0)}$ at the pump frequency ω_0 . The nonlinear coefficient is $\gamma = \frac{n_2 \omega_0}{c A_{\text{eff}}(\omega_0)}$, where n_2 is the nonlinear refractive index and c is the speed of light in vacuum, $A_{\text{eff}}(\omega_0)$ is the effective area of the mode at the pump frequency ω_0 , and $\alpha_2 = 9.3 \times 10^{-14}$ m/W is the two-photon absorption coefficient [12]. Finally the material response function includes both the instantaneous electronic response (Kerr type) and the delayed Raman response and has the form

$$R(t) = (1 - f_R) \delta(t) + f_R h_R(t), \quad (4)$$

$$h_R(t) = \frac{\tau_1^2 + \tau_2^2}{\tau_1 \tau_2} \exp\left(-\frac{t}{\tau_2}\right) \sin\left(\frac{t}{\tau_1}\right). \quad (5)$$

The f_R represents the fractional contribution of the delayed Raman response. The other parameters used for the simulation are listed in Table 2.

Table 2. Parameters used for simulation of the SC generation

Parameters	Waveguide length	Linear loss (α) [10, 15]	f_R [43]	τ_1 [43]	τ_2 [43]
Unit	cm	dB/cm	Null	fs	fs
Value	1	0.5	0.031	15.5	230.5

3. Numerical results

As the MIR SC generation requires the cladding as well as core materials of a waveguide to be transparent at long wavelengths, we first choose a channel waveguide fabricated using only chalcogenide materials with a rectangular core made of $\text{Ge}_{11.5}\text{As}_{24}\text{Se}_{64.5}$ glass and using $\text{As}_{36}\text{S}_{64}$ glass for both the upper and lower claddings, whose refractive index of 2.37 at 1.55 μm provides an index contrast of 0.3. By varying waveguide dimensions for realizing ZDW in the range of 2-4 μm or longer, we numerically calculated GVD for three different structures as a function of wavelength for the fundamental quasi-TE mode and plot them with material dispersion in Fig. 2. It can be observed from this figure that the material dispersion, shown by a

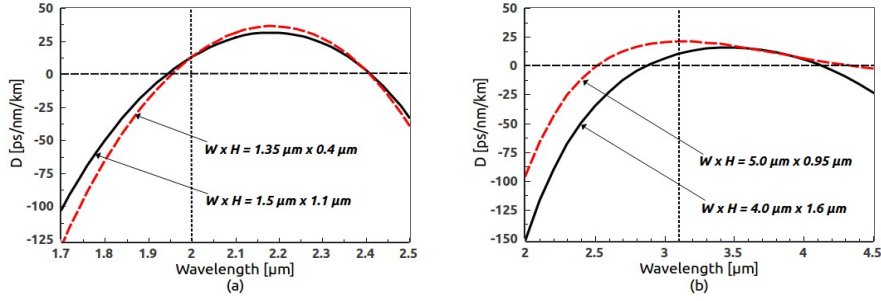


Fig. 3. GVD curves for the waveguide geometries employing two different lower claddings (solid black curve for $\text{Ge}_{11.5}\text{As}_{24}\text{S}_{64.5}$ and red dashed curve for MgF_2) for the fundamental quasi-TE mode (a) at a pump wavelength of $2 \mu\text{m}$ and (b) at a pump wavelength of $3.1 \mu\text{m}$. Vertical dotted line indicates the position of pump wavelength.

solid black line, remains normal for the wavelength range $1.5 \mu\text{m}$ to $5 \mu\text{m}$, considered here. The total dispersion curve for a waveguide with, $W = 4 \mu\text{m}$ and $H = 2.5 \mu\text{m}$ is shown by the green dot-dashed line, and it follows the material dispersion curve quite closely. As the waveguide dimension is reduced, waveguide dispersion becomes larger. However, total dispersion curves shown by red dotted and blue dashed lines for structures with, $W = 3.7 \mu\text{m}$, $H = 1.7 \mu\text{m}$ and $W = 1.7 \mu\text{m}$, $H = 1.7 \mu\text{m}$, respectively. After increasing the width and thickness of a structure to $W = 4.0 \mu\text{m}$ and $H = 2.5 \mu\text{m}$, total dispersion of the waveguide still remains normal ($-40 \text{ ps}/\text{nm}/\text{km}$) at $3.1 \mu\text{m}$ and continues to remain normal over a wide range of wavelengths exceeding $5 \mu\text{m}$. It appears unlikely that a waveguide can be designed to have anomalous dispersion in this wavelength range by employing such a lower index contrast cladding material such as $\text{As}_{36}\text{S}_{64}$ glass.

For realizing anomalous dispersion around the pump wavelength, cladding materials with larger index contrast than the $\text{As}_{36}\text{S}_{64}$ glass are required. To realize the ZDW between $2 \mu\text{m}$ and $4 \mu\text{m}$, we have chosen two different channel waveguides by replacing upper cladding with air and lower cladding with either $\text{Ge}_{11.5}\text{As}_{24}\text{S}_{64.5}$ glass or MgF_2 glass, respectively. With $\text{Ge}_{11.5}\text{As}_{24}\text{S}_{64.5}$ glass as the lower clad, index contrast increases to ~ 0.4 but with MgF_2 glass this value increases significantly to 1.3. To obtain the ZDWs of both designs close to the pump wavelength of $2 \mu\text{m}$ and to make GVDs slightly anomalous at these wavelengths, we optimized the dimensions of the waveguides. Similarly, another set waveguides were optimized for the longer pump wavelength of $3.1 \mu\text{m}$. Figures 3(a) and 3(b) show the GVD curves obtained for two different waveguide geometries optimized to work at the pump wavelengths of $2 \mu\text{m}$ and $3.1 \mu\text{m}$, respectively.

To study SC generation, we solve the generalized nonlinear Schrödinger equation (GNLSE) given in Eq. (3). We used the same computational method that was used in Karim *et al.* [8]. That study has indicated that there is a possibility to obtain spurious results if the adequate number of dispersion terms is not included during SC simulations. We solved Eq. (3) with the split-step Fourier method (SSFM) including up to 10^{th} order dispersion. We tested accuracy of the finite-element modal solution for a channel waveguide by a powerful extrapolation technique called Aitken's extrapolation [44]. We observed the convergence between the raw FEM results and extrapolated values as the number of FE elements increases along the transverse dimensions of the waveguide. We also tested the accuracy of numerically calculated GVD parameters for different number of elements used along the transverse dimensions of a channel waveguide. We fitted the dispersion data with a Taylor series expansion including up to 10^{th} order dispersion and found that this method accurately reproduced the GVD curves obtained by FE mode-solver

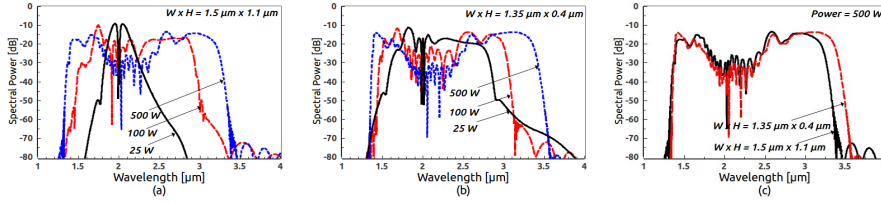


Fig. 4. Simulated SC spectra at a pump wavelength of $2 \mu\text{m}$ for (a) air-clad all-chalcogenide waveguide at peak power from 25, 100, and 500 W; (b) air-clad chalcogenide core employing MgF_2 for its lower cladding at the same power levels; (c) waveguides with two different lower claddings at a peak power of 500 W only.

over the whole wavelength range of calculations. A sufficiently small time step was chosen to accommodate the spectral expansion of the generated SC during numerical simulations.

We consider a waveguide containing a core of dimensions $W = 1.5 \mu\text{m}$ and $H = 1.1 \mu\text{m}$ with air and $\text{Ge}_{11.5}\text{As}_{24}\text{S}_{64.5}$ glass as upper and lower claddings, respectively. Another geometry has a core with $W = 1.35 \mu\text{m}$ and $H = 0.4 \mu\text{m}$ but MgF_2 glass as the lower cladding. Using FE mode-solver, we obtain $A_{\text{eff}} = 1.09 \mu\text{m}^2$ which yields $\gamma = 24.79 \text{ /W/m}$ for the structure with $\text{Ge}_{11.5}\text{As}_{24}\text{S}_{64.5}$ lower cladding and $A_{\text{eff}} = 0.51 \mu\text{m}^2$ which yields $\gamma = 53.39 \text{ /W/m}$ for the structure with MgF_2 lower cladding at a pump wavelength of $2 \mu\text{m}$. The GVD parameter calculated at the pump wavelength for both waveguides has a value of 13 ps/nm/km . These waveguides supported propagation of the fundamental TE mode up to the cut-off wavelength near $3.1 \mu\text{m}$ for the air-clad all-ChG structure and around $4 \mu\text{m}$ for the structure employing MgF_2 glass as lower cladding. A sech pulse of 150 fs duration (FWHM) was launched with peak power between 25 W and 500 W for numerical simulations. We included a wavelength-independent propagation loss of 2.5 dB/cm [10] for our 1-cm-long rectangular channel waveguides. Figure 4 shows the predicted SC spectra for the two waveguides at three different power levels at a pump wavelength of $2 \mu\text{m}$. In the case of 100 W input power the SC spectrum extends from $1.5 \mu\text{m}$ to around $3 \mu\text{m}$, producing a -30 dB bandwidth of 1500 nm for the waveguide using $\text{Ge}_{11.5}\text{As}_{24}\text{S}_{64.5}$ glass for its lower cladding. At the same power level the SC spectrum extends from $1.4 \mu\text{m}$ to around $3.1 \mu\text{m}$ producing a -30 dB bandwidth of 1700 nm for the waveguide with MgF_2 glass for its lower cladding. After increasing input peak power level at 500 W, the SC spectra broadened from $1.3 \mu\text{m}$ to $3.3 \mu\text{m}$ (output bandwidth of 2000 nm) and from $1.3 \mu\text{m}$ to $3.5 \mu\text{m}$ (output bandwidth of 2200 nm) for these two waveguides, respectively. The spectral evolution plots corresponding to Fig. 4(c) are shown in Fig. 5. It is apparent that a

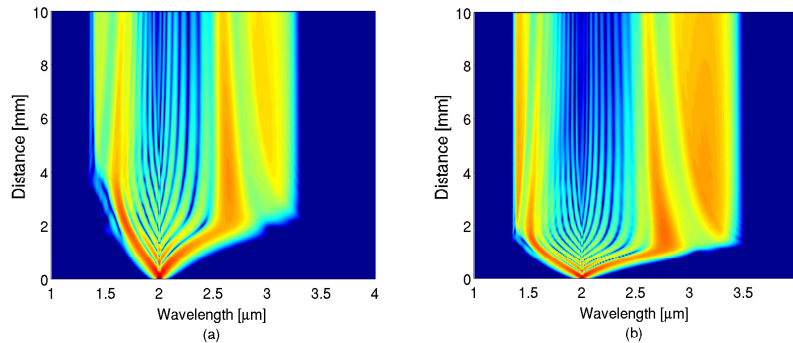


Fig. 5. Spectral evolution along the waveguide length corresponding to Fig. 4(c).

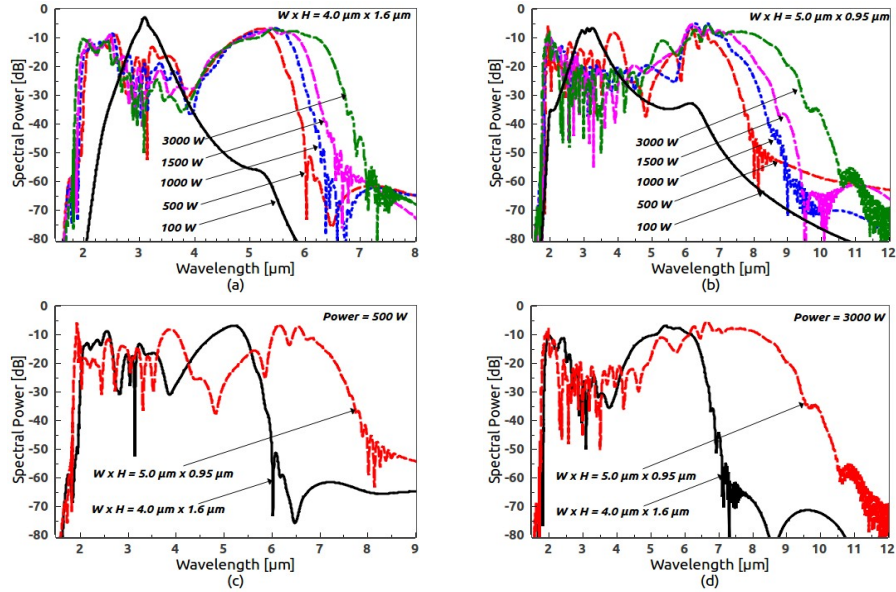


Fig. 6. Simulated SC spectra at a pump wavelength of $3.1 \mu\text{m}$ for (a) air-clad all-chalcogenide waveguide at peak power between 100 W and 3000 W; (b) air-clad chalcogenide core employing MgF_2 for its lower cladding for the same power levels; (c) waveguides employing with two different lower claddings at a peak power of 500 W only; (d) waveguides with two different lower claddings at peak power of 3000 W only.

larger output bandwidth can be realized by using a waveguide employing MgF_2 glass for its lower cladding. The reason behind this bandwidth enhancement solely related to the higher index contrast between the core and cladding materials when MgF_2 glass is used for the lower cladding. However, it was not possible to extend the SC spectrum to beyond $3.5 \mu\text{m}$ by using a pump wavelength of $2 \mu\text{m}$.

To extend the SC in the MIR regime, we need to shift the pump wavelength toward longer wavelengths [14]. We employ a pump wavelength of $3.1 \mu\text{m}$ since such a pump source has been realized at a repetition rate of 160 kHz [45]. Using 85 fs duration pulses at a wavelength of $3.1 \mu\text{m}$, we focus on a waveguide with $W = 4 \mu\text{m}$ and $H = 1.6 \mu\text{m}$ with $\text{Ge}_{11.5}\text{As}_{24}\text{S}_{64.5}$ glass for its lower lower cladding. The second waveguide structure had $W = 5 \mu\text{m}$ and $H = 0.95 \mu\text{m}$ but employed MgF_2 glass for its lower cladding. Using the FE mode-solver, we obtain $A_{\text{eff}} = 4.25 \mu\text{m}^2$ and $\gamma = 2.05 \text{ /W/m}$ for the first structure and $A_{\text{eff}} = 3.32 \mu\text{m}^2$ and $\gamma = 2.63 \text{ /W/m}$ for the second structure. The GVD parameter calculated at the pump wavelength for these waveguides has values of 10.22 ps/nm/km and 21 ps/nm/km, respectively. These waveguides supported propagation of the fundamental TE mode up to the cut-off wavelength around $6.5 \mu\text{m}$ for the air-clad all-ChG structure and beyond $12 \mu\text{m}$ for the structure employing MgF_2 as lower cladding.

After evaluating higher-order dispersion terms up to tenth-order from GVD curves shown in Fig. 3(b), we performed numerical simulations for SC generation in both the waveguide geometries at a power level between 100 W and 3000 W. The dispersion length, $L_D = T_p^2 / |\beta_2|$ for the 85 fs pump pulse for these two structures is 45 mm and 28 mm and the nonlinear length, $L_{\text{NL}} = 1/\gamma P$ at a peak power of 500 W is 0.98 mm and 0.76 mm, respectively. The soliton order, $N = \sqrt{L_D/L_{\text{NL}}}$ was 7 and 6 for the two waveguides, respectively, and the soliton fission length, $L_{\text{fiss}} \approx L_D/N$ was found to be 6.6 mm and 4.1 mm, respectively. Figure 6 shows the predicted

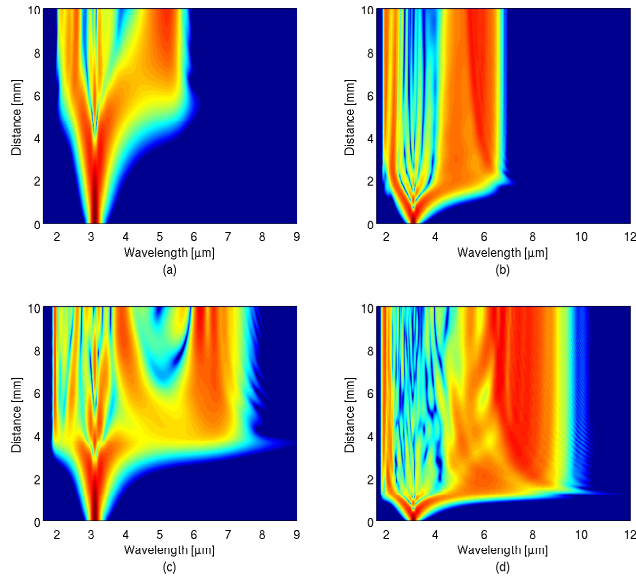


Fig. 7. Spectral evolution along the waveguide length corresponding to Fig. 6(c) (left column) and 6(d) (right column), respectively.

spectra at various power level up to 3000 W for the two waveguide geometries at a pump wavelength of $3.1 \mu\text{m}$. The spectral evolution plots corresponding to Fig. 6(c) and 6(d) are shown in Fig. 7. It is observed from Fig. 7 that the SC generation is dominated by soliton fission, which results in many short pulses generated through the soliton fission process whose spectra shifted towards the long wavelength side of the input spectrum. Raman-induced frequency shift (RIFS) is reducing gradually as solitons moved towards the second ZDWs located near $4.15 \mu\text{m}$ and $4.4 \mu\text{m}$ for the two waveguide geometries, respectively. Due to the spectral recoil effect [46, 47], RIFS were completely suppressed near the second ZDWs. At the same time, nonsolitonic radiation in the form of dispersive wave is produced at a wavelength that lies beyond the second ZDW. For the waveguide geometry employing $\text{Ge}_{11.5}\text{As}_{24}\text{S}_{64.5}$ glass as a lower cladding, it can be observed from Fig. 6 that the SC extends over $4 \mu\text{m}$ covering a wavelength range from $2 \mu\text{m}$ to $6 \mu\text{m}$ and for the structure employing MgF_2 as a bottom cladding, the SC extends over $6 \mu\text{m}$ covering a wavelength range from $1.8 \mu\text{m}$ to around $7.7 \mu\text{m}$ both at a peak power of 500 W. By increasing power level up to 3000 W, one can generate a SC spectrum that extends from $2 \mu\text{m}$ to $10 \mu\text{m}$ producing a bandwidth of $8 \mu\text{m}$ (> 2 octave) for the first waveguide and bandwidth of $9.2 \mu\text{m}$ (> 2.5 octave) for the second waveguide employing MgF_2 glass for its lower cladding.

There may be a disadvantage for ChG waveguides fabricated using MgF_2 glass for the lower cladding owing to its fragility. This problem becomes severe for long waveguides but is manageable for short waveguides around 1-cm-long [14]. Ma *et al.* [10] have shown experimentally that, if the top surface of the waveguides made from chalcogenide materials is left uncoated, the bare waveguide surface becomes rapidly contaminated by absorbing water and hydrocarbons from surrounding environment, resulting in increased losses. To prevent the surface contamination, a thin 10-nm protective coating layer of fluoro-polymer may be placed on top of the waveguide geometries proposed in this paper. We have tested numerically placing of such a thin

layer and found that the dispersions at a pump wavelength of $3.1 \mu\text{m}$ for the two waveguides used in our work was 9.85 ps/nm/km (10.23 ps/nm/km without coating) and 21.68 ps/nm/km (21 ps/nm/km without coating). Such relatively small changes in the β_2 value do not produce noticeable changes on the SC generated at the waveguide output.

Recently Yu *et al.* [15] proposed an air-clad rib waveguide whose core was made with $\text{Ge}_{11.5}\text{As}_{24}\text{Se}_{64.5}$ glass and whose lower cladding was made with $\text{Ge}_{11.5}\text{As}_{24}\text{S}_{64.5}$ glass. They were able to generate SC covering the wavelength range $1.8\text{-}7.5 \mu\text{m}$ when pumped with an optical parametric amplifier at $4 \mu\text{m}$ with a peak power of 3260 W . By rigorous numerical simulations, it is shown here that MIR SC can be generated with dispersion-engineered air-clad rectangular channel waveguide employing the same materials and covering the wavelength range of $1.9\text{-}7 \mu\text{m}$ by employing a pump source at a wavelength of $3.1 \mu\text{m}$ with a peak power of 3000 W . It is observed from Fig. 6 that MIR SC can be extended in the long wavelength regime up to $11 \mu\text{m}$ for a waveguide employing MgF_2 glass for its lower cladding when pumped with the same power and pump source although MgF_2 glass would be expected to absorb beyond $9 \mu\text{m}$ [10].

4. Conclusions

We have numerically demonstrated MIR SC generation by using dispersion-engineered, air-clad, channel waveguides designed and optimized such that they use either $\text{Ge}_{11.5}\text{As}_{24}\text{S}_{64.5}$ ChG glass or MgF_2 glass for its lower cladding material. The SC is generated with the waveguides proposed here by using pump pulses with low to moderate peak power at wavelength near $2 \mu\text{m}$ or $3.1 \mu\text{m}$. Although the nonlinear parameter has larger values at a pump wavelength of $2 \mu\text{m}$, the SC spectra were extended only over $1.3\text{-}3.3 \mu\text{m}$ and $1.3\text{-}3.5 \mu\text{m}$, respectively even at the highest but moderate peak power of 500 W for the two proposed structures. To extend SC to beyond the $5 \mu\text{m}$, it is necessary to choose a longer pump wavelength around $4\text{-}5 \mu\text{m}$. To realize the ZDW of the waveguide around this wavelength the core size of the waveguide must be increased which increases the effective mode area and hence reduces the nonlinear parameter. The only solution is to increase the peak power of the input pulse toward MW levels which can damage the input facet of the waveguide. Considering these factors, we designed and optimized air-clad two rectangular channel waveguides by employing two different lower cladding materials and choose $3.1 \mu\text{m}$ for the pump wavelength such that broadband SC could be generated at moderate peak power levels.

Using pump source at a wavelength of $3.1 \mu\text{m}$ with a relatively low peak power of 500 W we obtained a SC spectrum extended over 1.5 octave and covering the wavelength range from $2\text{-}6 \mu\text{m}$ with an air-clad all-ChG structure. However, when we used an optimized waveguide using MgF_2 glass for its lower cladding, the SC spectrum extended over more than two-octaves covered a wavelength range of $1.8\text{-}7.7 \mu\text{m}$. This, to the best of our knowledge, is the broadest MID SC at such a low peak power and at a lower pump wavelength of $3.1 \mu\text{m}$ using a chalcogenide waveguide. We have also found that, MIR SC can be extended over in the wavelength range $1.9\text{-}7 \mu\text{m}$ and $1.8\text{-}11 \mu\text{m}$ with a moderate peak power of 3000 W when the air-clad channel waveguide is designed with a $\text{Ge}_{11.5}\text{As}_{24}\text{Se}_{64.5}$ glass core and employs $\text{Ge}_{11.5}\text{As}_{24}\text{S}_{64.5}$ or MgF_2 glass for its lower cladding, respectively.